Journal of Materiomics xxx (xxxx) xxx

Contents lists available at ScienceDirect

Journal of Materiomics

journal homepage: www.journals.elsevier.com/journal-of-materiomics/

Opinion paper

Influence of Re-ions with different ionic radius in $Ba_{12}ReNb_9O_{36}$ on crystal structure and microwave dielectric properties

Pengcheng Zhang [a], Hao Li [a, *], Xiaoqing Chen [a], Xing Zhang [b, c], Hongcheng Yang [b, c], Canbing Li [a], Shuren Zhang [b, c]

[a] College of Electrical and Information Engineering, Hunan University, Changsha, 410082, China
[b] State Key Laboratory of Electronic Thin Films and Integrated Devices, University of Electronic Science and Technology of China, Chengdu, 610054, China
[c] National Engineering Research Center of Electromagnetic Radiation Control Materials, University of Electronic Science and Technology of China, Chengdu, 610054, China

ARTICLE INFO

Article history:
Received 13 September 2020
Received in revised form
16 April 2021
Accepted 4 May 2021
Available online xxx

Keywords:
Microwave dielectric ceramic
$Ba_{12}ReNb_9O_{36}$
Polarizability
Raman spectrum

ABSTRACT

The $Ba_{12}ReNb_9O_{36}$ (Re=Yb, Ce, Tm, Er, Y, Ho, Dy, Gd) ceramics are synthesized by solid-phase reaction method. The phase composition, crystal structure, microstructure, and microwave dielectric properties of the ceramics are investigated by X-ray diffraction, X-ray photoelectron spectroscopy, Scanning electron microscopy and Raman spectrum. The optimal microwave dielectric properties (ε_r = 37.23, Q × f = 36600 GHz, and τ_f = 34 ppm/°C) are obtained for $Ba_{12}YbNb_9O_{36}$ ceramic sintered at 1420 °C for 6 h. In this system, the variation of dielectric constant is dominated by polarizability. The Q × f is mainly affected by internal strain/fluctuation of d-spacing. The variation of τ_f is related to the temperature coefficient of dielectric constant and the oxygen octahedron distortion. Furthermore, the reduction of Ce^{4+} ions, the relative density, linear thermal expansion coefficient, and the second phase are also important factors affecting microwave dielectric properties.

1. Introduction

Over decades, microwave dielectric ceramics (MWDCs) have attracted substantial attention in the wake of the booming development of aerospace, internet of things, communication, medical, and automotive drive [1]. MWDCs have been used to fabricate filters, transmission lines, resonators, and oscillators commercially [2]. In order to obtain materials with a suitable dielectric constant (ε_r), low dielectric loss (Q = 1/tanδ) and near-zero temperature coefficient of resonant frequency (τ_f), researchers have conducted extensive investigations on microwave dielectric ceramics and focused on revealing the relationship between preparation process, structure, and properties.

Ceramics with a perovskite structure have been receiving much attention. As an important member of the perovskite family, the hexagonal perovskite has a wide application potential in various fields, such as oxide ion conducting materials, photoluminescence materials, and magnetic oxides [3–5]. Interestingly, the hexagonal perovskite also shows reliable microwave dielectric properties. In MWDCs, the hexagonal perovskite mainly includes: $A_nB_nO_{3n}$, $A_nB_{n-1}O_{3n}$ and $A_nB_{n-2}O_{3n}$. Low-loss microwave dielectric materials (i) $A_nB_nO_{3n}$ such as $Ba_3(B'Ta_2)O_9$ (B′ = Mg and Zn) [6,7], $Ba_4(LiTa_2Sb)O_{12}$ [8], and $Ba_4(LiTa_3)O_9$ [9] ceramics and (ii) $A_nB_{n-1}O_{3n}$ such as $SrLa_4Ti_4O_{15}$ [10], $Ba_8(MTa_6)O_{24}$ (M = Co, Ni, Zn) [11,12], and $Ba_8(MNb_6)O_{24}$ (M = Ni, Zn) [13,14] ceramics have been reported. However, few works on $A_nB_{n-2}O_{3n}$ typological compounds were reported. Therefore, this paper focuses on the study of hexagonal perovskite with the general formula $A_nB_{n-2}O_{3n}$.

For complex perovskite ceramics with the formula of $A^{2+}(B'^{1+}_{1/4}B'^{5+}_{3/4})O_3$, using trivalent ions to completely replace the monovalent ions at the B′-site is reckon as a reasonable method to synthesize hexagonal perovskite ($A^{2+}(B'^{3+}_{1/12}B'^{5+}_{3/4})O_3$, or $A_{12}B'B''_9O_{36}$) with $A_nB_{n-2}O_{3n}$ type. Based on this, $Ba_{12}B'Nb_9O_{36}$ ceramics is designed to understand the effect of trivalent cation substitution at the B′-site on the $Ba_4(B'^{+})Nb_3O_{12}$ compound. According to previous work, doping rare earth (Re) element into ceramic system has been illustrated to be valid for improving microwave dielectric properties, such as $Ca_{0.66}Ti_{0.66}R_{0.34}Al_{0.34}O_3$ (Re= La, Sm, Nd), and $ReVO_4$ (Re = Nd, Sm) systems, etc [15,16]. Besides,

* Corresponding author.
E-mail address: hli@hnu.edu.cn (H. Li).
Peer review under responsibility of The Chinese Ceramic Society.

https://doi.org/10.1016/j.jmat.2021.05.001

Please cite this article as: P. Zhang, H. Li, X. Chen *et al.*, Influence of Re-ions with different ionic radius in $Ba_{12}ReNb_9O_{36}$ on crystal structure and microwave dielectric properties, Journal of Materiomics, https://doi.org/10.1016/j.jmat.2021.05.001

in $RETiTaO_6$ (RE = La, Ce, Pr, Nd, Sm, Eu, Gd, Tb, Dy, Ho, Y, Er, Yb) and $SrRE_4Si_3O_{13}$ (RE = La, Pr, Nd, Sm, Eu, Gd, Tb, Dy, Er, Tm, Yb, and Y) systems, the introduction of rare earth ions with different radius is helpful to modify the temperature coefficient [17,18]. In this work, the $Ba_{12}ReNb_9O_{36}$ (Re=Yb, Ce, Tm, Er, Y, Ho, Dy, Gd) ceramics are synthesized by solid-phase reaction method, and the relationship between structure and microwave dielectric properties is investigated systematically.

2. Experimental

The solid-state reaction method is carried out to prepare $Ba_{12}ReNb_9O_{36}$ ceramics. The starting raw $BaCO_3$ (99%, aladdin), Nb_2O_5 (99%, aladdin), Re_xO_y (99%) (Yb_2O_3, CeO_2, Tm_2O_3, Er_2O_3, Y_2O_3, Ho_2O_3, Dy_2O_3, Gd_2O_3, Nanjing Reagent) are weighed by stoichiometry. These powders are ground for 4 h in a ball grinder with 220-rotate speed by blending zirconia balls and ethyl alcohol. Then, dried (85 °C) and sieved (60-mesh) mixtures are calcined at 1100 °C for 4 h. The powders are re-milled, dried, and granulated with 5 wt% polyvinyl alcohol. After being pressed into cylinders at 20 MPa. The specimens are sintered at 1400°C–1500 °C for 6 h.

The $Ba_{12}ReNb_9O_{36}$ phase is checked by an X-ray diffraction (Philips x'pert Pro MPD, Netherlands) instrument with CuKα radiation. The network analyzer (Agilent Technologies E5071C, the USA) is performed to measure microwave dielectric properties based on the Hakki-Coleman dielectric resonator method [19]. Ceramic morphologies are obtained by scanning electron microscopy (SEM). The Raman spectra (50-900 cm^{-1}) are obtained by a Raman spectrometer (RENISHAW, London, UK), and the existing line is He–Ne laser at 514 nm. Thermal expansion data are tested by using a thermal analyzer (NETZSCH STA449C). Room temperature X-ray photoelectron spectroscopy (XPS) are executed, a step of 0.1 eV, using the Al Kα (nonmonochromatic) radiation of an Escalab 250Xi (Thermo Fisher Scientific) spectrometer operated in the fixed analyzer transmission. The Archimedes method is implemented to measure bulk density. The τ_f value is obtained by the following formula [20]:

$$\tau_f = \frac{f_{85} - f_{25}}{f_{25}(85-25)} \times 10^6 (\mathrm{ppm}/^\circ C) \quad (1)$$

where f_{25} and f_{85} are the resonant frequency at 25 °C and 85 °C, respectively.

3. Results and discussion

3.1. Phase composition and crystal structure

The $Ba_{12}ReNb_9O_{36}$ (Re=Yb, Ce, Tm, Er, Y, Ho, Dy, Gd) ceramics are prepared *via* traditional solid-phase reaction method. The X-ray diffraction patterns of $Ba_{12}ReNb_9O_{36}$ ceramics with different Re ions sintered at 1400–1500 °C are shown in Fig. 1(a). The diffraction peaks of $Ba_{12}ReNb_9O_{36}$ (Re= Yb, Ce, Tm, Er, Y, Ho, Dy) are well matched with the standard card ($Ba_4Lu_{1/3}Nb_3O_{12}$: JCPDS #76–0014). Ba_2GdNbO_6 (JCPDS #24–1142) phase appeared after introducing Gd ions. As shown in Fig. 1(b), the diffraction peak corresponding to (110) lattice plane shifts toward low angle with the increase of ion radius, illustrating the increase of cell volume. However, there is an abnormal phenomenon for $Ba_{12}CeNb_9O_{36}$ ceramic, as displayed in Fig. 1(b) with the blue part. It may be caused by the reduction of partial Ce^{4+} ions (CN = 6, R = 0.87 Å) to Ce^{3+} ions (CN = 6, R = 1.01 Å) at high temperature. Based on this speculate, X-ray photoelectron spectroscopy (XPS) measurement was adopted for etched surfaces of $Ba_{12}CeNb_9O_{36}$ ceramic. The survey spectrum in Fig. 2(a) indicates the presence of Ba, Ce, Nb, O,

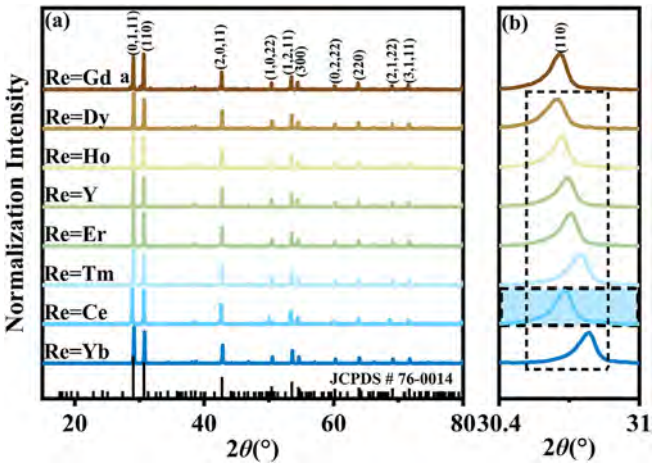

Fig. 1. (a) XRD diagrams of $Ba_{12}ReNb_9O_{36}$ (Re=Yb, Ce, Tm, Er, Y, Ho, Dy, Gd) ceramic sintered at 1400–1500 °C for 4h; (b) XRD diffraction profile at *hkl* = 110 in the region of 2θ = 30–31.2°.

and C from contamination carbon. As seen in Fig. 2(b)–(d), The peaks located at 778.7 eV and 794.3 eV are assigned to Ba 3d of Ba^{2+} ions [21,22]. The Nb^{5+} ions of $3d_{3/2}$ and $3d_{5/2}$ spin-orbital splitting photoelectrons are located at 205.7 and 208.5 eV, respectively [23]. The characteristic XPS signals of Ce^{3+} $3d_{5/2}$, and Ce^{4+} $3d_{5/2}$ electronic states are observed at 881 eV, 885 eV, and 888.6 eV, respectively. The three peaks at 899.1 eV, 902.9 eV, and 904.8 eV are assigned to Ce^{3+} $3d_{3/2}$, and Ce^{4+} $3d_{3/2}$, respectively. The result is consistent with the analysis reported by Eric and Janek *et al.* (Ce^{3+} $3d_{5/2}$: 880.9 ± 0.2 eV, 885.2 ± 0.2 eV, Ce^{4+} $3d_{5/2}$: 888.6 ± 0.2 eV) [24,25]. The analysis confirms that Ce^{4+} ions are reduced to Ce^{3+}, and the mechanism of Ce^{4+} ion reduction can be described as:

$$O_o \rightarrow V_o^{\cdot\cdot} + 2e' + \frac{1}{2}O_2 \quad (2)$$

$$Ce^{4+} + e' \rightarrow Ce^{3+} \quad (3)$$

The Rietveld refinement is carried out to verify the variation of lattice parameters. The refined result of $Ba_4Yb_{1/3}Nb_3O_{12}$ ceramic is presented in Fig. 3(a) as an example. The discrepancy factors of R_p, R_{wp}, and χ [2] are 7.65%, 5.21% and 4.324, respectively. The structure parameters of $Ba_{12}YbNb_9O_{36}$ ceramic are calculated as a = b = 5.825 Å, c = 42.605 Å, and the cell volume V = 1251.883 $Å^3$. Refined results of $Ba_{12}ReNb_9O_{36}$ ceramics are listed in Table 1. The crystal structure obtained by refinement is shown in Fig. 3(b). The cell parameters as a function of ionic radius are depicted in Fig. 3(c)–(e). As the ionic radius increases from 0.868 Å to 0.938 Å, the lattice parameters a, b, c, and cell volume gradually increase. According to the Bragg's equation (2dsinθ = λ) of the hexagonal system and the relationship between d-spacings and indices of crystal face, the mechanism of diffraction peak shifting can be described as:

$$\sin^2\theta = \frac{\lambda^2}{4}\left(\frac{4}{3}\frac{h^2+hk+k^2}{a^2} + \frac{l^2}{c^2}\right) \quad (4)$$

Based on Equation (4), the θ of the (110) diffraction peak is inversely proportional to the lattice parameter of a. Thus, the (110) diffraction peak shifts to the low angle. Furthermore, the calculated lattice parameter a = 5.834 Å of $Ba_{12}CeNb_9O_{36}$ ceramic is less than that of $Ba_{12}DyNb_9O_{36}$ ceramic and larger than that of $Ba_{12}HoNb_9O_{36}$, corresponding to the shift of $Ba_{12}CeNb_9O_{36}$ ceramic with (110) diffraction peak.

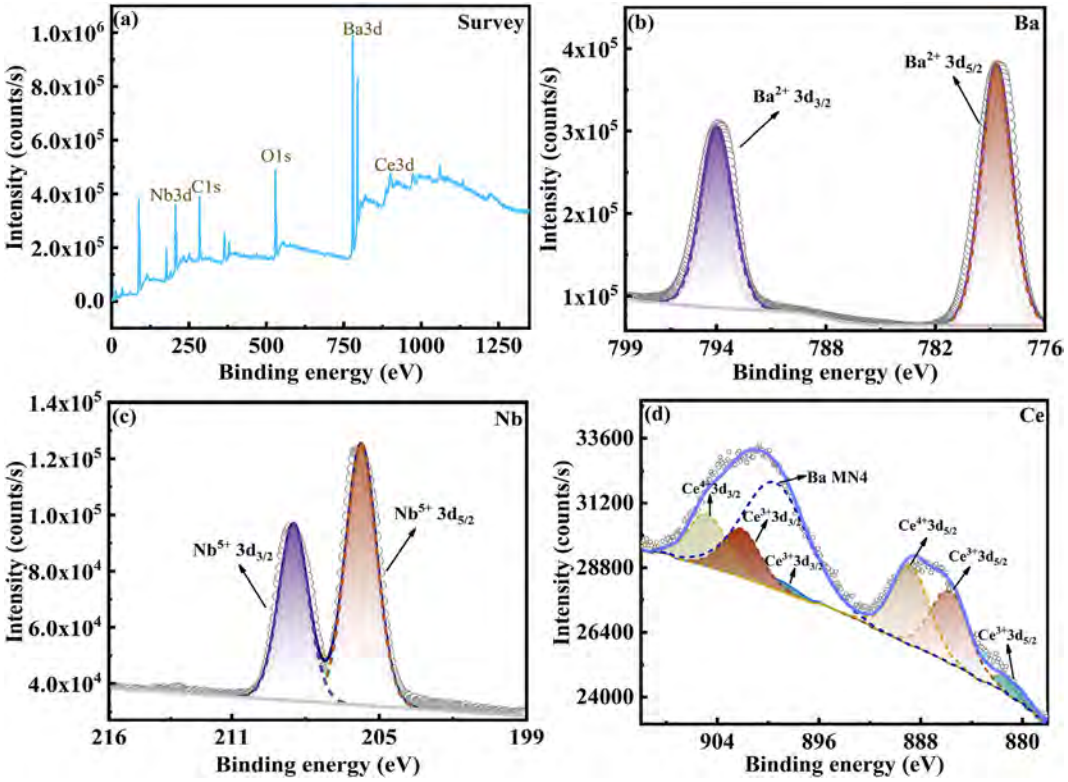

Fig. 2. XPS spectra of $Ba_{12}CeNb_9O_{36}$ ceramic with (a) the survey spectrum and high-resolution spectra of (b) Ba 3d, (c) Nb 3d, and (d) Ce 3d.

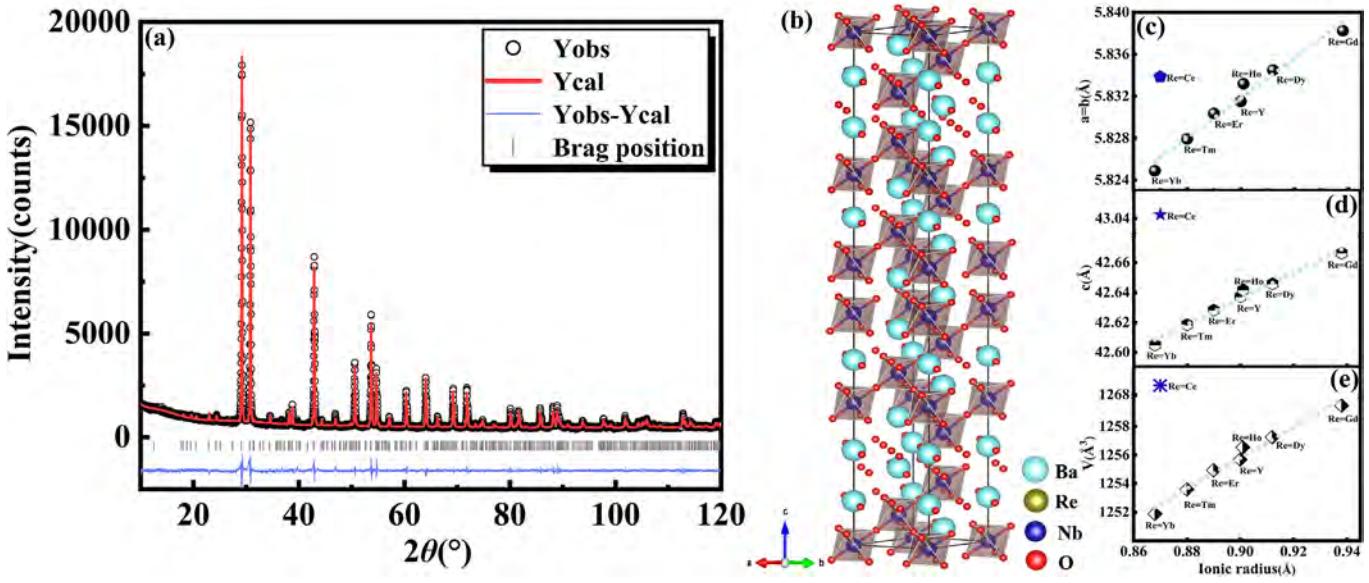

Fig. 3. (a) Rietveld refinement pattern of $Ba_{12}YbNb_9O_{36}$ ceramic sintered at 1420 °C; (b) the crystal structure of the $Ba_{12}ReNb_9O_{36}$ ceramic; the variation of lattice parameters a = b (c), c (d) and cell volume V (e) with ion radius from 0.868 Å to 0.938 Å.

3.2. Microstructure and microwave dielectric properties

The SEM analysis is performed to investigate the surface micromorphology. Fig. 4 describes the microstructure of $Ba_{12}ReNb_9O_{36}$ ceramics sintered at optimal sintering temperature (the sintering temperature corresponds to the maximum Q × f values). The $Ba_{12}ReNb_9O_{36}$ ceramics with Re=Yb, Ce, Tm, Y, Ho, Dy, Gd show a compact microstructure with an average grain size of 4–9 μm. The relative density values of those ceramics are listed in Table 2, which is consistent with the observed microstructures.

Table 1
Rietveld refinement information of the $Ba_{12}ReNb_9O_{36}$ ceramics with different ionic radius.

$Ba_{12}ReNb_9O_{36}$	R(Å)	a = b(Å)	c(Å)	Vol(Å^3)	Re−O(Å)	Rwp(%)	Rp(%)	χ [2]
Re = Yb	0.868	5.825	42.605	1251.883	2.05521	7.65	5.21	4.324
Re = Ce	0.870	5.834	43.043	1268.644	2.06397	5.7	4.36	2.482
Re = Tm	0.880	5.828	42.618	1253.594	2.05579	7.38	5.36	3.902
Re = Er	0.890	5.830	42.628	1254.923	2.05652	6.28	4.68	2.971
Re = Y	0.900	5.831	42.637	1255.677	2.05693	6.38	4.69	3.095
Re = Ho	0.901	5.833	42.642	1256.537	2.0574	6.44	4.84	3.028
Re = Dy	0.912	5.835	42.646	1257.244	2.05778	6.75	4.84	3.291
Re = Gd	0.938	5.838	42.666	1259.443	2.05899	6.27	4.67	2.974

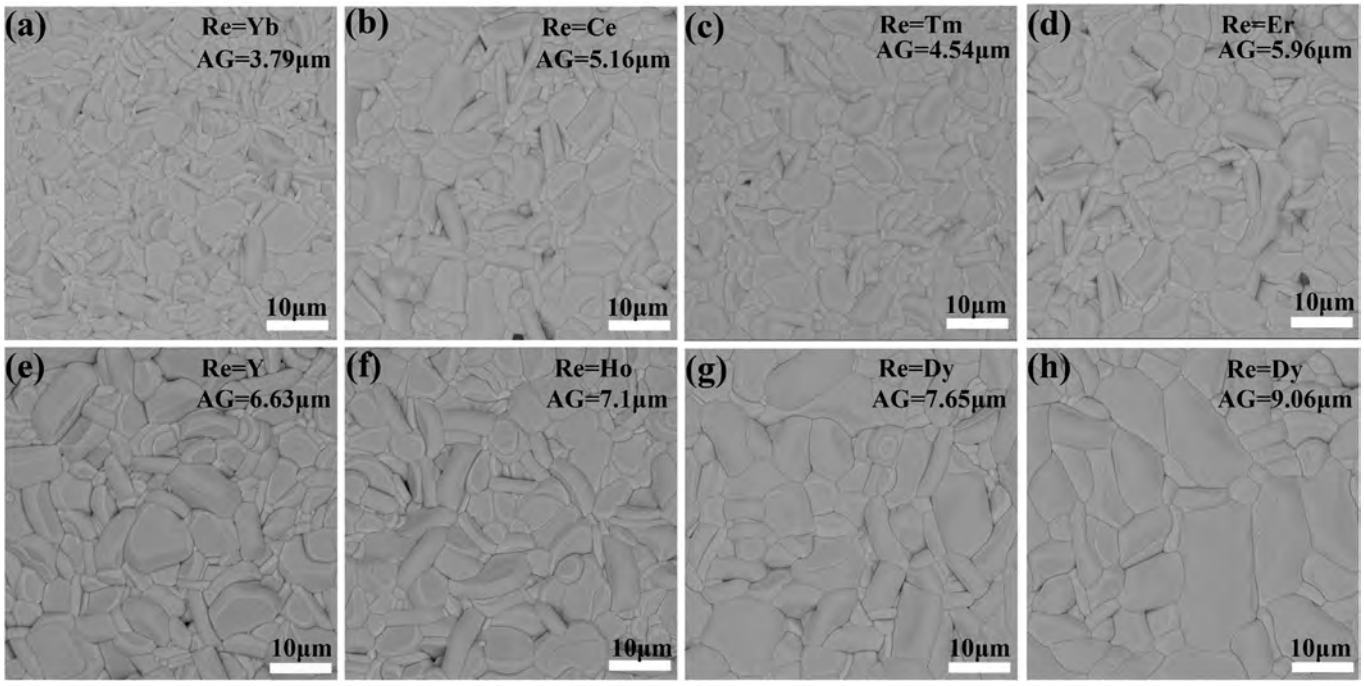

Fig. 4. SEM images of (a) $Ba_{12}YbNb_9O_{36}$, (b) $Ba_{12}CeNb_9O_{36}$, (c) $Ba_{12}TmNb_9O_{36}$, (d) $Ba_{12}ErNb_9O_{36}$, (e) $Ba_{12}YNb_9O_{36}$, (f) $Ba_{12}HoNb_9O_{36}$, (g) $Ba_{12}DyNb_9O_{36}$, and (h) $Ba_{12}GdNb_9O_{36}$ ceramics sintered at optimum temperature for 4 h.

Table 2
Bulk density, theory density, and relative density of $Ba_{12}ReNb_9O_{36}$ ceramics sintered at 1420−1490 °C.

$Ba_{12}ReNb_9O_{36}$	ST(°C)	ρ1 (g/cm^3)	ρ2 (g/cm^3)	RD (%)
Re = Yb	1420	6.181	6.432736	96.087
Re = Ce	1490	5.881	6.214332	94.636
Re = Tm	1420	6.094	6.415798	94.989
Re = Er	1455	5.974	6.405679	93.258
Re = Y	1440	5.991	6.246408	95.916
Re = Ho	1420	6.112	6.392835	96.381
Re = Dy	1470	6.218	6.384425	97.393
Re = Gd	1435	6.250	6.362894	98.226

ST: sintering temperature, **ρ1:** bulk density.
ρ2: theory density, **RD:** relative density.

3.3. The relationship between structure and microwave dielectric properties

The permittivity represents the polarization ability of materials under the electric field [26]. At microwave frequency, the polarization is derived from electron displacement polarization and ionic displacement polarization, where ion displacement polarization plays a major role in the dielectric constant. Shannon *et al.* [27]. suggested that molecular polarizability can be estimated as the sum of individual ionic polarizabilities, which can be obtained as follows in this system:

$$\alpha_D = 12\alpha\left(Ba^{2+}\right) + \alpha\left(Re^{3+}\right) + 9\alpha\left(Nb^{5+}\right) + 36\alpha\left(O^{2-}\right) \quad (5)$$

where ions polarizability can be obtained by R. D. Shannon [28]. The relationship between polarizability and dielectric constant are shown in Fig. 5. In general, the dielectric constant and the polarizability of $Ba_{12}ReNb_9O_{12}$ ceramics exhibit an increasing trend as the polarizability of doped Re ions increases. However, with the same theoretical α = 188.7 Å^3 value, $Ba_{12}ErNb_9O_{36}$ ceramics show an anomalous decrease compared that of $Ba_{12}YNb_9O_{36}$ ceramics. This phenomenon is related to the lower relative density of $Ba_{12}ErNb_9O_{12}$ (93.3%) ceramics compared to $Ba_{12}YNb_9O_{36}$ (95.9%) ceramics, which leads to the lower ε_r for $Ba_{12}ErNb_9O_{36}$ ceramics. The ε_r values of $Ba_{12}TmNb_9O_{36}$ and $Ba_{12}YNb_9O_{36}$ ceramics are almost equal, which may be related to the nearly equal polarization α_D = 188.7 Å^3 and similar sintering characteristic of them. The

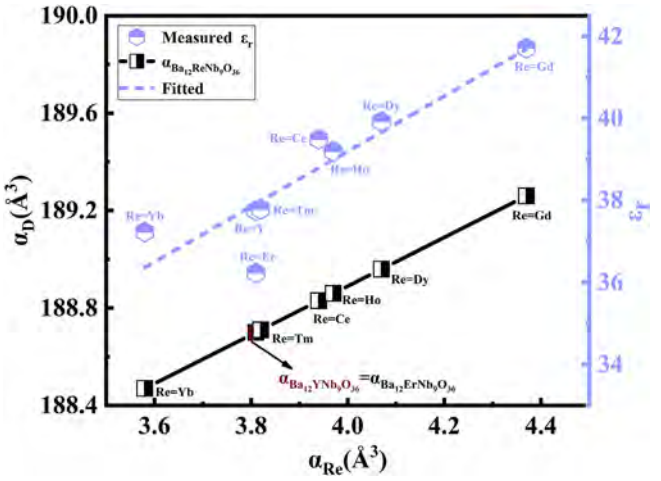

Fig. 5. (a) The dielectric constant and ionic polarizability of $Ba_{12}ReNb_9O_{36}$ ceramics.

highest dielectric constant of $Ba_{12}GdNb_9O_{36}$ ceramic also stemmed from the effect of second phase ($Ba(Gd_{1/2}Nb_{1/2})O_3$: $\varepsilon_r = 40$, $Q \times f = 5700$ GHz, and $\tau_f = 4.6$) [29]. Although the polarizability of $Ba_{12}HoNb_9O_{36}$ ceramic is larger than $Ba_{12}CeNb_9O_{36}$, the ε_r of $Ba_{12}HoNb_9O_{36}$ ceramic is less than that of $Ba_{12}CeNb_9O_{36}$ ceramic. It can be explained by the increased polarizability due to the reduction of partial Ce ions ($\alpha(Ce^{3+}) = 6.15$ Å^3>$\alpha(Ho^{3+}) = 3.97$ Å^3). The detailed results with permittivity and polarizability are summarized in Table 3.

The microwave dielectric loss is determined by the external and internal factors. External factors are related to grain boundary and pores. Internal factors originated from lattice vibrational anharmonicity [30]. The Re-site of $Ba_{12}ReNb_9O_{36}$ ceramics occupies by using rare earth ions with various ionic radius, the and $Q \times f$ varies from 9477 GHz to 36600 GHz, as displayed in Table 4. Thus, can be surmised that the ionic radius plays a dominate role in the dielectric loss. According to Hitoshi Ohsato et al., the differences of $Q \times f$ values of each ceramics may be related to internal strain/fluctuation of d-spacing η. It is reported that the low internal η value leads to a low dielectric loss in $Ba_{6-3x}R_{8+2x}Ti_{18}O_{54}$ (R = La, Pr, Nd, Sm) systems [31]. Thus, the variation internal strain/fluctuation of d-spacing in $Ba_{12}ReNb_9O_{36}$ systems is evaluated by the following equation proposed by Stokes and Wilson [32].

$$\beta = 2\eta \cdot \tan\theta \quad (6)$$

where β is the full width at half maximum (FWHM) of the X-ray diffraction peaks and θ is the diffraction angle. The β value is chosen from the strongest peaks in XRD patterns. As shown in Fig. 6, the η value increases with the increase of ion radius. The variation of $Q \times f$ and η values show a an opposite trend. The larger η value indicates that the structure tends to be unstable [33]. Thus, the unstable structure influences the $Q \times f$ values. The $Q \times f$ of $Ba_{12}CeNb_9O_{36}$ ceramic decreases sharply, which relates to the reduction of Ce^{4+} ions. Similar phenomenon is found in Ti-based ceramics [34]. Furthermore, the low relative density of $Ba_{12}ErNb_9O_{36}$ ceramic, and the second phase ($Ba(Gd_{1/2}Nb_{1/2})O_3$: $Q \times f = 5700$ GHz) of $Ba_{12}GdNb_9O_{36}$ ceramic also affect dielectric

Table 3
Dielectric constant and polarizability of $Ba_{12}ReNb_9O_{36}$ ceramics at various Re ions.

$Ba_{12}ReNb_9O_{36}$	α_{Re} (Å^3)	ε_r	α_D (Å^3)
Re=Yb	3.58	37.23	188.47
Re=Er	3.81	39.49	188.7
Re=Y	3.81	37.78	188.7
Re=Tm	3.82	36.23	188.71
Re=Ce	3.94	37.75	188.83
Re=Ho	3.97	39.19	188.86
Re=Dy	4.07	39.92	188.96
Re=Gd	4.37	41.71	189.26

Table 4
The $Q \times f$ value and internal strain/fluctuation of d-spacing of $Ba_{12}ReNb_9O_{36}$ ceramics at various Re ions.

$Ba_{12}ReNb_9O_{36}$	R(Å) (CN = 6)	$Q \times f$ (GHz)	FWHM	tanθ	η
Re=Yb	0.868	36600	0.142	0.5579	0.1273
Re=Ce	0.87	23995	0.147	0.5520	0.1332
Re=Tm	0.88	27271	0.146	0.5576	0.1309
Re=Er	0.89	24250	0.148	0.5574	0.1328
Re=Y	0.9	24048	0.153	0.5571	0.1373
Re=Ho	0.901	19085	0.154	0.5570	0.1383
Re=Dy	0.912	14588	0.165	0.5560	0.1484
Re=Gd	0.938	9477	0.173	0.5589	0.1548

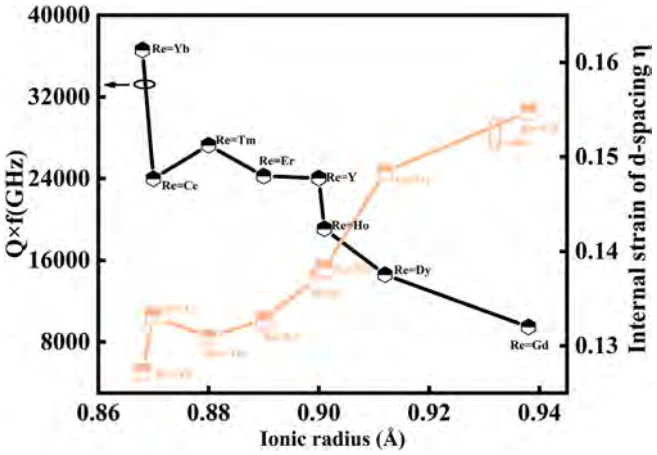

Fig. 6. The relationship between $Q \times f$ and internal strain of d-spacing for $Ba_{12}ReNb_9O_{36}$ ceramics with ionic radius from 0.868 Å to 0.938 Å.

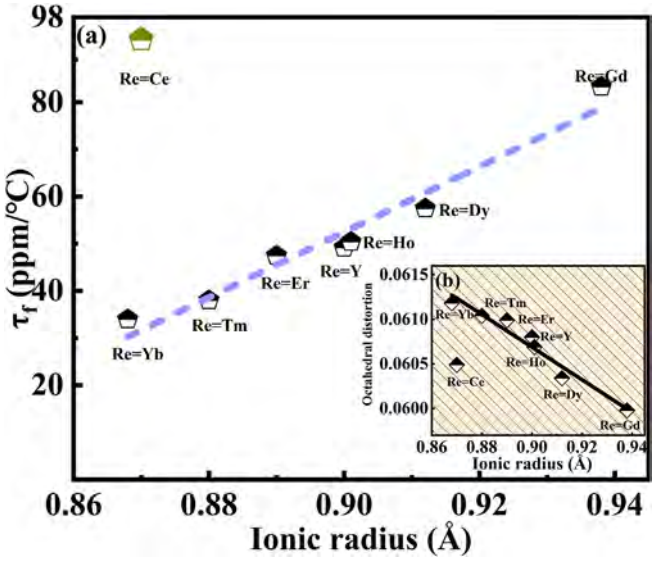

Fig. 7. (a) The variation of τ_f value in $Ba_{12}ReNb_9O_{36}$ ceramics with ionic radius from 0.868 Å to 0.938 Å; (b) The relationship between τ_f and oxygen octahedron distortion.

Table 5
The τ_f, oxygen octahedron distortion, α_L, and τ_ε of $Ba_{12}ReNb_9O_{36}$ ceramics at various Re ions.

$Ba_{12}ReNb_9O_{36}$	R(Å) (CN = 6)	τ_f (ppm/°C)	$\Delta_{distortion}$ ($\times 10^{-2}$)	α_L (ppm/°C)
Re=Yb	0.868	34.0	6.118	10.56
Re=Tm	0.88	38.0	6.104	9.96
Re=Er	0.89	47.5	6.099	11.73
Re=Y	0.9	49.2	6.080	12.44
Re=Ho	0.901	50.4	6.069	12.33
Re=Dy	0.912	57.5	6.034	11.16
Re=Gd	0.938	83.3	5.998	11.92
Re=Ce	0.87	93.3	6.049	12.15

Table 6
Character table of irreducible representations of $Ba_{12}ReNb_9O_{36}$ structure.

D_{3d}(3 m)	E	$2C_3$	$3C_2$	i	$2S_6$	$3\sigma_d$	Selection rules
$\mathbf{A_{1g}\Gamma_1^+}$	1	1	1	1	1	1	$\alpha_{xx}+\alpha_{yy}$, α_{zz}
$\mathbf{A_{1u}\Gamma_1^-}$	1	1	1	−1	−1	−1	
$\mathbf{A_{2g}\Gamma_2^+}$	1	1	−1	1	1	−1	R_z
$\mathbf{A_{2u}\Gamma_2^-}$	1	1	−1	−1	−1	1	T_z
$\mathbf{E_g\Gamma_3^+}$	2	−1	0	2	−1	0	(R_x, R_y)(α_{xx}-α_{yy}, α_{xy}), (α_{xz}, α_{yz})
$\mathbf{E_u\Gamma_3^-}$	2	−1	0	−2	1	0	(T_X,T_y)

Table 7
Raman and IR vibrational modes of $Ba_{12}ReNb_9O_{36}$ ceramic.

Atom	Position	Symmetry	Irreducible vibrational representations
Nb1	6c	C_{3V}	$A_{2u} + E_u + A_{1g} + E_g$
Nb2	6c	C_{3V}	$A_{2u} + E_u + A_{1g} + E_g$
Re1	6c	C_{3V}	$A_{2u} + E_u + A_{1g} + E_g$
Ba1	6c	C_{3V}	$A_{2u} + E_u + A_{1g} + E_g$
Ba2	6c	C_{3V}	$A_{2u} + E_u + A_{1g} + E_g$
Ba3	6c	C_{3V}	$A_{2u} + E_u + A_{1g} + E_g$
Nb3	3a	D_{3d}	$A_{2u} + E_u$
Re2	3a	D_{3d}	$A_{2u} + E_u$
O1	18h	Cs	$2A_{2u}+3E_u+2A_{1g}+3E_g + A_{1u} + A_{2g}$
O2	18h	Cs	$2A_{2u}+3E_u+2A1_g+3E_g + A_{1u} + A_{2g}$
O3	18h	Cs	$2A_{2u}+3E_u+2A_{1g}+3E_g + A_{1u} + A_{2g}$

$\Gamma_{acoustic} = A_{2u} + E_u$.
$\Gamma_{optic} = 12A_{1g}+3A_{1u}+3A_{2g}+13A_{2u}+16E_u+15E_g$.
Raman active modes: $12A_{1g}+15E_g+3A_{2g}$.
Infrared active modes: $13A_{2u} + 16E_u$.

losses. The detailed Q × f and η are summarized in Table 4.

The τ_f increases gradually when the ionic radius of doped rare earth increases, as displayed in Fig. 7(a). In this paper, the B′-site (oxygen octahedron) is substituted by different Re ions, which leads to the different degree of distortion. The distortion factor is calculated by the bond length [35].

$$\Delta = \frac{1}{6}\sum\left(\frac{R_i - R_A}{R_A}\right)^2 \quad (7)$$

where R_i and R_A are the individual bond length and average bond length, which are obtained from Rietveld Refinement. The oxygen octahedron distortion shows an inverse change compared to that of τ_f value, as shown in Fig. 7(b). This result is consistent with that reported by Tang *et al.* in the $Ca_{0.61}Nd_{0.26}Ti_{1-x}(Cr_{0.5}Nb_{0.5})_xO_3$ ceramic [34]. The decrease of octahedral distortion stems from the decline of restoring forces between the cation and oxygen, which subsequently leads to the increase of temperature coefficient [35]. The detailed τ_f and oxygen octahedron distortion are listed in Table 5. According to Bosman *et al.* [36]., the τ_f value obeys:

$$\tau_f = -\left(\alpha_L + \frac{1}{2}\tau_\varepsilon\right) \quad (8)$$

where α_L and τ_ε represent linear thermal expansion coefficient and temperature coefficient of dielectric constant, respectively. Based on this, the α_L and τ_ε values were measured to explain the variation of temperature coefficient of resonant frequency. The measured α_L values are shown in Fig. S1(a)–(h), in which α_L varies in range of 9.96–12.44 ppm/°C. The results are in accordance with Zhou *et al.* who reported that the α_L of MWDCs is relatively small (<+20 ppm/°C) [36]. Therefore, the τ_f is mainly influenced by the τ_ε. As the τ_f increases, the τ_ε gradually decreases, showing an opposite trend, as presented in Fig. S2. The results indicated that the variation of τ_f can also be evaluated by the τ_ε.

3.4. Raman spectroscopy and vibrational mode analysis

Raman spectroscopy is an effective method to determine phase composition, analyze lattice vibration and build structure-property relationships [37]. The irreducible representations containing the

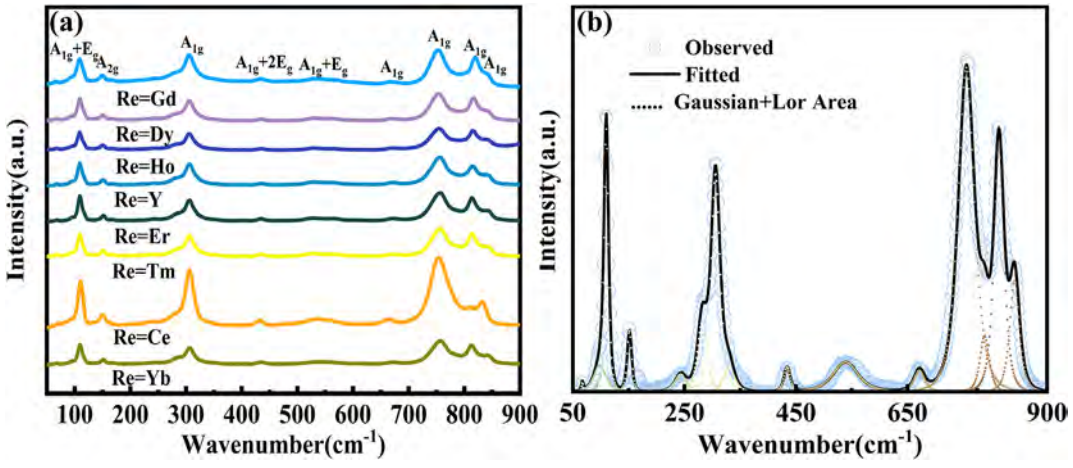

Fig. 8. (a) Raman spectra of $Ba_{12}ReNb_9O_{36}$ (Re=Yb, Ce, Tm, Er, Y, Ho, Dy, Gd) ceramics sintered at optimal temperatures. (b) The measured (circle) and fitted (black solid line) Raman spectra of $Ba_4Yb_{1/3}Nb_3O_{12}$ ceramics based on Gaussian + Lor Area model.

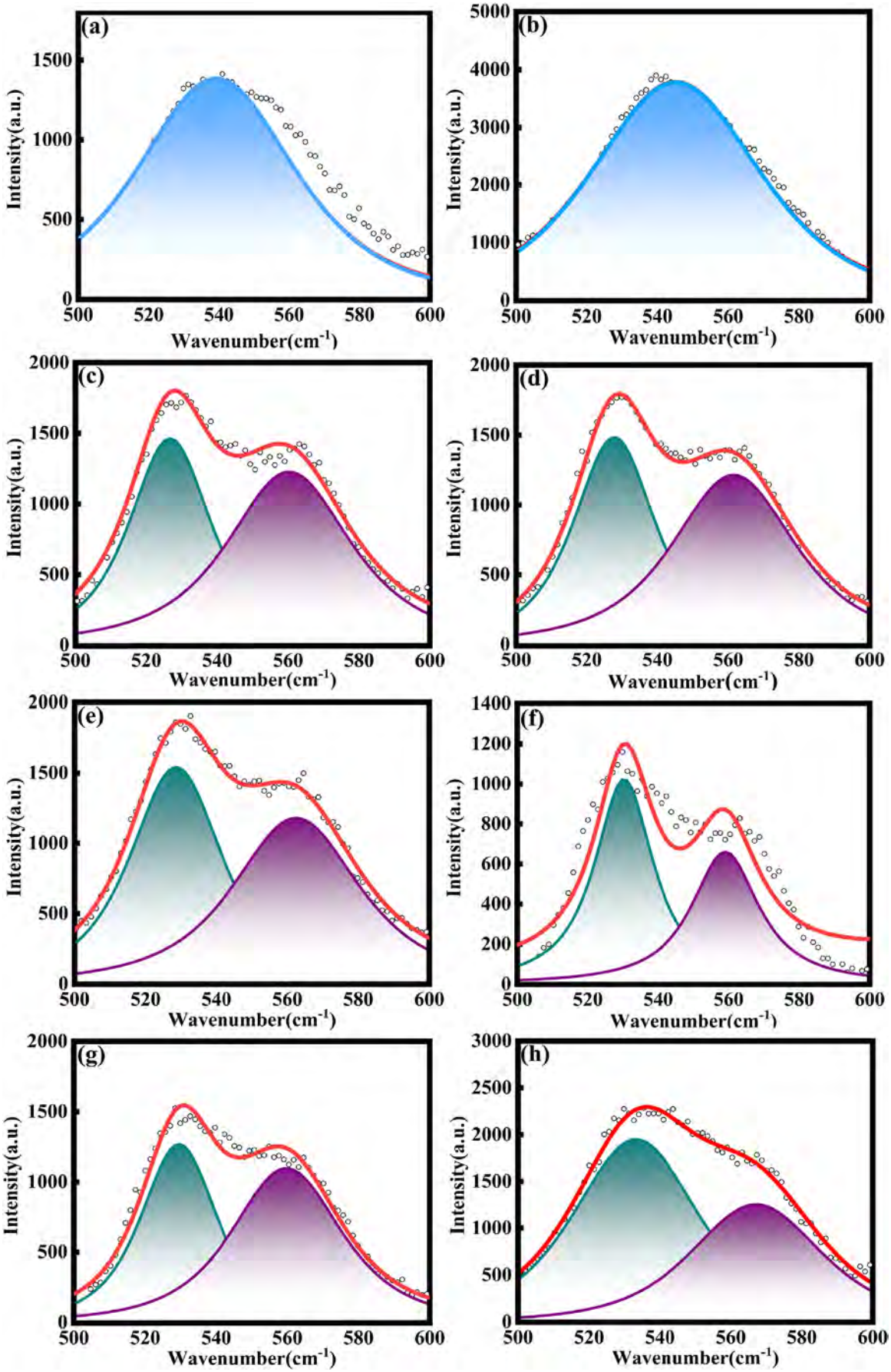

Fig. 9. The measured and fitted Raman spectra at 500-600 cm^{-1} of (a) $Ba_{12}YbNb_9O_{36}$, (b) $Ba_{12}CeNb_9O_{36}$, (c) $Ba_{12}TmNb_9O_{36}$, (d) $Ba_{12}ErNb_9O_{36}$, (e) $Ba_{12}YNb_9O_{36}$, (f) $Ba_{12}HoNb_9O_{36}$, (g) $Ba_{12}DyNb_9O_{36}$, and (h) $Ba_{12}GdNb_9O_{36}$ ceramics.

selection rule of crystalline material can be determined by point group analysis, as listed in Table 6. According to Bilbao crystallographic server [38], the acoustic and optic vibrational representation for hexagonal phase is $12A_{1g}+3A_{1u}+3A_{2g}+13A_{2u}+16E_u+15E_g$. Classified infrared Raman active modes with $Ba_{12}ReNb_9O_{36}$ are summarized in Table 7.

Each Raman mode is related to the displacement of each ions originated from lattice vibration in the structure. The Raman peak at 110 cm^{-1} can be assigned to $A_{1g} + E_g$ modes, corresponding to Nb−O octahedral vibration (NbO_6) and Ba−O bond vibration [39]. The Raman peak at 151 cm^{-1} is named as A_{2g} modes. The A_{1g} (Nb−O vibration) mode at 306 cm^{-1} has been identified as the ordered structure-related vibrations [40]. The internal vibrations of oxygen octahedra and oxygen-octahedron stretch mode are located in 435 cm^{-1} ($A_{1g}+2E_g$) and 756 cm^{-1} (A_{1g}), respectively [40,41]. The weak bands at 500-600 cm^{-1}, which are related to Ba ($A_{1g} + E_g$) and Ba−O (A_{1g}) vibrations (translational motions), are insensitive to chemical substitution on B-sites [42].

The Raman spectra with the assigned modes of $Ba_{12}ReNb_9O_{36}$ ceramic are shown in Fig. 8(a). As the increase of ionic radius, the A_{1g} mode corresponding to B-site vibration at 306 cm^{-1} moves to the low wavenumber. All Raman profiles are fitted by the Gaussian + Lorentz Area, and in Fig. 8(b), $Ba_4Yb_{1/3}Nb_3O_{12}$ ceramic was taken as an example. An intense peak exists in the fitted spectrum of $Ba_{12}ReNb_9O_{36}$ (Re═Yb, Ce) ceramic at 500-600 cm^{-1}, however, the split mode at Re═Tm, Er, Y, Ho, Dy, Gd is observed, as presented in Fig. 9. The phenomenon may be related to the difference of Re and Nb ions in electronegativity and ionic radius. The larger discrepancy in electronegativity and ionic radius is easy to form the split mode [43].

4. Conclusion

The crystal structure, phase composition, microstructure, and structure-property relationship of $Ba_{12}ReNb_9O_{36}$ ceramics are investigated systematically. The XRD pattern and the Rietveld refinement indicate that pure $Ba_{12}ReNb_9O_{36}$ (Re═Yb, Ce, Tm, Er, Y, Ho, Dy) ceramics with hexagonal structure are obtained. There existed the second phase Ba_2GdNbO_6 for $Ba_{12}GdNb_9O_{36}$ ceramic. With the increase of ionic radius, the cell volume gradually increases. However, the reduction of Ce^{4+} ions leads to an abnormal increase of cell volume for $Ba_{12}CeNb_9O_{36}$ ceramic. The ε_r, Q × f, and τ_f separately vary in the range of 36.23−41.71, 9477−36600 GHz, and 34−93.3 ppm/°C when the ionic radius changes from 0.868 to 0.938 Å. The optimal microwave dielectric properties (ε_r = 37.23, Q × f = 36600 GHz, τ_f = 34 ppm/°C) of $Ba_{12}ReNb_9O_{36}$ ceramics sintered at 1420 °C for 6 h are obtained when Re ions is Yb.

Declaration of competing interest

The authors declare that they have no known competing financial interests or personal relationships that could have appeared to influence the work reported in this paper.

Appendix A. Supplementary data

Supplementary data to this article can be found online at https://doi.org/10.1016/j.jmat.2021.05.001.

References

[1] Guo HH, Zhou D, Pang LX, Qi ZM. J Eur Ceram Soc 2019;39:2365−73. https://doi.org/10.1016/j.jeurceramsoc.2019.02.010.
[2] Fan J, Zhao Q, Du K, Wang F, Wang XH, Lu WZ, et al. J Am Ceram Soc 2020;103:3231−7. https://doi.org/10.1111/jace.17016.
[3] Fop S, McCombie KS, Wildman EJ, Skakle JMS, McLaughlin AC. Chem Commun (Camb). 2019;55:2127−37. https://doi.org/10.1039/c8cc09534e.
[4] Yang HY, Li QF, Liu ZH. Mod Phys Lett B 2017;31:15854−64. https://doi.org/10.1142/s0217984917503237.
[5] Yin WG, Liu X, Tsvelik AM, Dean MPM, Upton MH, Kim J, et al. Phys Rev Lett 2013;111:057202. https://doi.org/10.1103/PhysRevLett.111.057202.
[6] Kawashima S, Nishida M, Ueda I. Ouchi★ H. 1983;66:421−3. https://doi.org/10.1111/j.1151-2916.1983.tb10074.x.
[7] Nomura S, Toyama K, Kaneta K. Jpn J Appl Phys 1982;21:L624−6. https://doi.org/10.1143/jjap.21.l624.
[8] Tang Y, Fang L, Su C, Zhang H. Ceram Int 2014;40:7633−6. https://doi.org/10.1016/j.ceramint.2013.12.077.
[9] Fang L, Li C, Peng X, Hu C, Wu B, Zhou H. J Am Ceram Soc 2010;93:1229−31. https://doi.org/10.1111/j.1551-2916.2009.03548.x.
[10] Jawahar IN, Santha NI, Sebastian MT, Mohanan P. J Mater Res 2002;17:3084−9. https://doi.org/10.1557/JMR.2002.0446.
[11] Thirumal M, Davies PK. J Am Ceram Soc 2005;88:2126−8. https://doi.org/10.1111/j.1551-2916.2005.00426.x.
[12] Kan A, Ogawa H, Yokoi A, Ohsato H. Jpn J Appl Phys 2006;45:7494−8. https://doi.org/10.1143/jjap.45.7494.
[13] Lu F, Wang X, Pan Z, Pan F, Chai S, Liang C, et al. Dalton Trans 2015;44:13173−85. https://doi.org/10.1039/c5dt00859j.
[14] Tao F, Wang X, Gong M, Lu F, Allix M, Kuang X, et al. J Am Ceram Soc 2017;100:1212−20. https://doi.org/10.1111/jace.14601.
[15] Li W, Fang L, Sun Y, Tang Y, Chen J, Li C. J Electron Mater 2016;46:1956−62. https://doi.org/10.1007/s11664-016-5179-9.
[16] Xu Y, Fu R, Agathopoulos S, Wang X, Yang Y, Cai J. J Alloys Compd 2017;693:454−61. https://doi.org/10.1016/j.jallcom.2016.09.226.
[17] Thomas S, Sebastian MT. J Am Ceram Soc 2009;92:2975−81. https://doi.org/10.1111/j.1551-2916.2009.03326.x.
[18] Surendran KP, Solomon S, Varma MR, Mohanan P, Sebastian MT. J Mater Res 2011;17:2561−6. https://doi.org/10.1557/jmr.2002.0372.
[19] Hakki BW, Coleman PD. IRE Transactions on Microwave Theory and Techniques 1960;8:402−10. https://doi.org/10.1109/TMTT.1960.1124749.
[20] Zhang J, Zuo R. J Am Ceram Soc 2017;100:5249−58. https://doi.org/10.1111/jace.15077.
[21] Chen X, Li H, Zhang P, Hu H, Tao Y, Li G. J Am Ceram Soc 2021:1−10. https://doi.org/10.1111/jace.17762. 00.
[22] Meshesha DS, Matangi RC, Tirukkovalluri SR, Bojja S. S Afr J Chem Eng 2017;23:10−6. https://doi.org/10.1016/j.sajce.2016.10.004.
[23] Hryniewicz T, Rokosz K, Sandim HRZ. SEM/EDX and XPS studies of niobium after electropolishing. Appl Surf Sci 2012;263:357−61. https://doi.org/10.1016/j.apsusc.2012.09.060.
[24] Bêche E, Charvin P, Perarnau D, Abanades S, Flamant G. Surf Interface Anal 2008;40:264−7. https://doi.org/10.1002/sia.2686.
[25] Hartmann P, Brezesinski T, Sann J, Lotnyk A, Eufinger J-P, Kienle L, et al. ACS Nano 2013;7:2999−3013. https://doi.org/10.1021/nn400255w.
[26] Song XQ, Xie MQ, Du K, Lu W-Z, Lei W. Journal of Materiomics 2019;5:606−17. https://doi.org/10.1016/j.jmat.2019.07.005.
[27] Shannon RD, Subramanian MA, Allik TH, Kimura H, Kokta MR, Randles MH, et al. J Appl Phys 1990;67:3798−802. https://doi.org/10.1063/1.345026.
[28] Shannon RD. Dielectric polarizabilities of ions in oxides and fluorides. J Appl Phys 1993;73:348−66. https://doi.org/10.1063/1.353856.
[29] Abdul Khalam L, Sreemoolanathan H, Ratheesh R, Mohanan P, Sebastian MT. Mater Sci Eng, B 2004;107:264−70. https://doi.org/10.1016/j.mseb.2003.11.019.
[30] Yang H, Zhang S, Yang H, Zhang X, Li E. Inorg Chem 2018;57:8264−75. https://doi.org/10.1021/acs.inorgchem.8b00873.
[31] Ohsato H. J Eur Ceram Soc 2007;27:2911−5. https://doi.org/10.1016/j.jeurceramsoc.2006.11.044.
[32] Stokes AR, Wilson AJC. Proc Phys Soc 1944;56:174−81. https://doi.org/10.1088/0959-5309/56/3/303.
[33] Zhang X, Tang B, Fang Z, Yang H, Xiong Z, Xue L, et al. Inorganic Chemistry Frontiers 2018;5:3113−25. https://doi.org/10.1039/c8qi00956b.
[34] Li H, Zhang P, Yu S, Yang H, Tang B, Li F, et al. Ceram Int 2019;45:11639−47. https://doi.org/10.1016/j.ceramint.2019.03.037.
[35] Xiong Z, Yang C, Tang B, Fang Z, Chen H, Zhang S. Ceram Int 2018;44:7384−92. https://doi.org/10.1016/j.ceramint.2017.12.186.
[36] Bosman AJ, Havinga EE. Phys Rev 1963;129:1593−600. https://doi.org/10.1103/PhysRev.129.1593.
[37] Guo H-H, Zhou D, Pang L-X, Qi Z-M. J Eur Ceram Soc 2019;39:2365−73. https://doi.org/10.1016/j.jeurceramsoc.2019.02.010.
[38] Kroumova E, Aroyo MI, Perez-Mato JM, Kirov A, Capillas C, Ivantchev S, et al. Phase Transitions 2003;76:155−70. https://doi.org/10.1080/0141159031000076110.
[39] Wang CH, Jing XP, Wang L, Lu J. J Am Ceram Soc 2009;92:1547−51. https://doi.org/10.1111/j.1551-2916.2009.03067.x.
[40] Dong HL, Shi F. Appl Spectrosc Rev 2011;46:207−21. https://doi.org/10.1080/05704928.2010.538459.
[41] Surendran KP, Sebastian MT, Mohanan P, Moreira RL, Dias A. Chem Mater 2005;17:142−51. https://doi.org/10.1021/cm048411s.
[42] Dias A, Khalam LA, Sebastian MT, Paschoal CWA, Moreira RL. Chem Mater 2006;18:214−20. https://doi.org/10.1021/cm051982f.
[43] Ramarao SD, Murthy VRK. Dalton Trans 2015;44:2311−24. https://doi.org/10.1039/c4dt02364a.

Pengcheng Zhang is currently pursuing his Ph.D. degree in the College of Electrical and Information Engineering, Hunan University, Changsha, China. His current research interest focuses on microwave dielectric ceramics.

Hao Li is an associate professor in the College of Electrical and Information Engineering, Hunan University, Changsha, China. He received his Ph.D. degree from University of Electronic Science and Technology of China. His research interests include microwave dielectric materials and devices for microwave communication.